Thermal Stability of Sol−Gel-Derived Porous AM-Al$_x$Zr Mixed Oxides

Jens Klein and Wilhelm F. Maier*

Max-Planck-Institut für Kohlenforschung, Kaiser-Wilhelm-Platz 1 D-45470 Mülheim, Ruhr, Germany

Received May 11, 1999. Revised Manuscript Received June 21, 1999

The thermal stability of the Al−Zr mixed oxides has been studied over the whole range of composition. The effect of temperature treatment on porosity, crystallinity, and microstructure has been investigated (Ar adsorption isotherms, HR-TEM, EDX, XRD, DRIFTS). The effect of impregnation and doping on the temperature stability of these oxides is shown. An amorphous porous Al−Zr mixed oxide, stabilized with 5% Si oxide and whose microstructure is stable up to 1400 °C with no indication of phase separation or nanocrystal formation, was prepared. The study shows, that amorphous mixed oxides may be a promising new approach to the development of high-temperature stable porous materials.

Introduction

Conventional thermal combustion, as practiced in fossil fuel based power plants, has as its major drawback the unavoidable thermal NO_x formation. Due to the more stringent emission standards,[1] huge efforts are necessary to remove this NO_x from the exhaust gas before it is released into the environment. Thus catalytic NO_x removal has become a major cost factor for today's fossil fuel based power plants. It is therefore very attractive, to find concepts to avoid the formation of NO_x rather than to allow its formation and then remove it afterward at high cost. Such a concept is the catalytic combustion as a promising alternative to thermal combustion. By reducing the operating temperature catalytic combustion reduces significantly the thermal NO_x formation as most attractive advantage. In addition a higher fuel conversion efficiency can be obtained.[2] However, this feature can only be utilized, if the combustion reaction can be restricted to the catalyst surface, flame formation must be prevented by the design of the catalytic burner. This requires highly active combustion catalysts of high surface area and high thermal stability. While the former is available in great abundance, there are no catalyst materials of sufficient thermal stability known to date.

During the last 15 years increasing attention to catalytic combustion can be recognized.[3−7] However, due to a lack of temperature stable catalysts, the investigations of catalytic combustion at temperatures of 1000 °C or higher have been very limited. Although most hydrocarbons are readily oxidized at such temperatures, complete combustion of residual hydrocarbon traces at high conversion levels is much more affected by mass transfer limitations of the reactants to the active surface than by the activity of each active site.[8] In the context of desired material properties, thermal and mechanical stability are the most significant parameters. Generally the most often used materials in industrial applications are alumina, silica, zirconia, or titania. More academic still, but promising, are also perovskites, hexaaluminates, and spinels.[9] The catalysts presently used for catalytic combustion (i.e., methane combustion in natural gas) are noble metals (Pt, Pd, or Rh) deposited on alumina.[6] Catalyst poisoning is not a problem at the high temperatures employed in catalytic combustion. At combustion operating temperatures, typical catalyst poisons are volatile and do not form stable compounds with the catalyst.[10] Catalysts operating at such high temperatures do not lose activity by active site poisoning, but rather by a drastic decrease of pore volume and surface area and encapsulation of the catalytically active site (metal) due to sintering processes.[10] For a combustion catalyst operated at high space velocity, a large surface area, stable even at high temperatures, is the central factor to maintain high conversions at short contact times. Main goal for the development of better combustion catalysts is therefore the improvement of the thermal stability of a porous microstructure of the catalyst.

Alumina and zirconia are commonly used support materials in heterogeneous catalysis, whereby zirconia is chemically more stable than alumina or silica.[11] In the vicinity of 1000 °C and especially in the presence of steam, the specific surface area of alumina strongly decreases in association with its transformation to the α phase.[12] Zirconia shows a similar behavior, but in another temperature range: it transforms at around

(1) Cusumano, J. A. *CHEMTECH* **1992**, *8*, 482.
(2) Eguchi, K.; Arai, H. *Catal. Today* **1996**, *29*, 379.
(3) Nakajima, H. I. *Catal. Today* **1996**, *29*, 109.
(4) Arai, H.; Fukuzawa, H. *Catal. Today* **1995**, *26*, 217.
(5) Beguin, B.; Garbowski, E.; Peter, S. D.; Primet, M. *React. Kinet. Catal. Lett.* **1996**, *59*, 253.
(6) Trimm, D. L. *Catal. Today* **1995**, *26*, 231.
(7) Machida, M.; Eguchi, K.; Arai, H. *J. Catal.* **1987**, *103*, *487*.
(8) Prasad, R.; Kennedy, L. A.; Ruckenstein, E. *Catal. Rev.-Sci. Eng.* **1984**, *26*, 1.
(9) Ismagilov, Z. R. *Catal. Rev. − Sci. Eng.* **1990**, *32*, 51.
(10) Pfefferle, L. d.; Pfefferle, W. C. *Catal. Rev. − Sci. Eng.* **1987**, *29*, 219.
(11) Lin, Y.-S.; Chang, C.-H.; Gopalan, R. *Ind. Eng. Chem. Res.* **1994**, *33*, 860.

10.1021/cm990280l CCC: $18.00
Published on Web 08/07/1999

600 °C to the thermodynamically stable monoclinic phase.[12] Sintering of small particles or amorphous regions can already start at temperatures 0.3−0.5 times of the melting point, which is 2045 °C for alumina (α phase) and 2300 °C for zirconia. Very little is known about mixed Al−Zr oxides, especially with respect to porosity and thermal stability.

A common approach to stabilize porous surfaces is the introduction of a third component such as La^{3+}, Y^{3+}, Ce^{3+}, Ba^{2+}, or Ca^{2+} aimed to suppress sintering processes and to maintain a stable surface area. The effect of additives is studied over a broad range of elements in the periodic table.[4,7,13−22] Much effort has been devoted to the study of support stabilization (i.e., alumina and zirconia) undoped and doped with La^{3+}, Y^{3+}, Ce^{3+}, Si^{4+}, or alkali metals.[13] The stabilization of Al_2O_3 by ZrO_2 has been studied and improved mechanical properties such as strength and toughness of these materials have been recognized.[13] We report here about our studies on the preparation, microstructure, and thermal stability of $Al_2O_3 - ZrO_2$ mixed oxides over the whole composition range.

Experimental Section

Synthesis. The samples were prepared by a modified sol−gel process with the metal alkoxide precursors $Al(O^{sec}Bu)_3$ and $Zr(O^nPr)_4$ and 4-hydroxy-4-methyl-pentadione as stabilizer to avoid precipitation.

The molar ratio alkoxides:water:acid (HCl):complexing agent: alcohol (^{i}PrOH) was 1:1:0.06:3:65. The Al/Zr ratio was varied from 0, 0.01, 0.5, 0.1 to 0.95, 0.99, 1.

After the alkoxide mixture with the hydroxy-substituted pentadione was stirred for 1 h in a 100-mL polypropylene beaker, 30 mL of 2-propanol was added and the solution was stirred for another 30 min. Then a mixture of 20 mL of alcohol, water, and acid was added at once under continuous stirring.

The gelation time strongly depends on the alumina content. With a high amount (>60%) of Al_2O_3, gelation occurs after 1−10 min, while the pure zirconia gels needed up to 10 days for gelation. The color change of the gels from colorless to orange strongly depends on the alumina-content. All samples were calcined after drying in the hood as follows:

$$\mathrm{RT} \xrightarrow{(0.2°/\mathrm{min})} 65\ °\mathrm{C}/5\ \mathrm{h} \xrightarrow{(0.2°/\mathrm{min})} 250\ °\mathrm{C}/5\ \mathrm{h} \xrightarrow{(2°/\mathrm{min})} \mathrm{RT}$$

These materials were then heated to higher calcination temperatures according to the following temperature program:

$$\mathrm{RT} \xrightarrow{(2°/\mathrm{min})} x°\mathrm{C}/2\ \mathrm{h} \xrightarrow{(2°/\mathrm{min})} \mathrm{RT}$$

where x = 500 °C, 750 °C, 1000 °C, 1250 °C. The incorporation of a third component as stabilizer was achieved by dissolving the acetylacetonate of the component in the desired amount in the above mixture of alkoxides and alcohol during the initial sol−gel preparation. The rest of the procedure remained as described above. The gelation time was found to increase with the amount of the additive.

For the impregnation by incipient wetness method, the same acetylacetonate salt was dissolved in 10 mL of alcohol and 20 μL of hydrochloric acid and the already calcined material of choice was stirred in this solution for 12 h. In the case of Si^{4+} the calcined material was stirred with a solution of TEOS ($Si(OEt)_4$) in 2-propanol. After filtration, the impregnated material was dried in air at room temperature and calcined afterward at 600 °C for 5 h.

Characterization. The surface areas were determined by single point BET (SORPTY 1750, FISONS); argon physisorption was obtained with a SORPTOMATIK 1990 (FISONS) in liquid argon (−186 °C).

The DSC measurements were performed with a DSC 50 (SHIMADZU) with a heating rate of 10 °C/min.

X-ray powder diffraction (XRD) patterns were measured in the Debye−Scherrer technique on a STOE STADI 2/PL diffractometer using Cu Kα radiation in the range of 2θ =10−80°. The detector used was an area detector PSD 1. The temperature dependence of the patterns was examined in the temperature range from 50 to 900 °C (stepwise increase by 50 K prior to each measurement) and displayed after background correction.

Spectral properties of the materials were examined with FTIR spectroscopy in diffusive reflectance (DRIFTS) using a BRUKER IFS 48 spectrometer equipped with a HARRICK−DRIFTS unit DRA in combination with the high vacuum chamber (HVC). The ground samples were diluted with KBr and the mixture was dried in situ in a flow of argon at 773 K. The spectra were collected with a spectral resolution of 2 cm^{-1} (200 scans), and the experimental data displayed using the Kubelka−Munk function (dry KBr as background) at 400 °C under flowing argon.

The solid-state NMR measurements were obtained at a MSL-300 spectrometer (BRUKER) with an optimal contact time of 0.5−0.7 μs and π/2 pulses. The spinning rate was between 3 and 6 kHz. The external standard was the zeolite Na−Y with a chemical shift $\delta(^{27}Al)$ = 62.8 ppm.[23]

HRTEM. Selected AM materials have been examined with high-resolution transmission electron microscopy (HRTEM) on a HITACHI HF 2000 instrument combined with energy-dispersive X-ray analysis (EDX). Microstructure was investigated by electron diffraction (magnification 200k; camera length 0.2 m) and high-resolution imaging, while elemental distribution was investigated by selected area EDX microanalyses with area sizes varying from 2 nm to several micrometers. The samples were crushed in an agate mortar in a methanol suspension and transferred to a Holey carbon grid (copper, 3 mm diameter).

Results and Discussion

The materials have been prepared by a modified, acid-catalyzed sol−gel process. Emphasis was paid to a homogeneous behavior of the sol−gel transition. Reaction conditions have been adjusted until phase separations, opalescence, and precipitation phenomena could be avoided.

preparation reaction:

$$a\mathrm{M}'(\mathrm{OR})_x + b\mathrm{M}(\mathrm{OR}')_y + \mathrm{H_2O} \rightarrow \mathrm{MM}'\mathrm{O}_z + ax\mathrm{ROH} + by\mathrm{R}'\mathrm{OH}$$

with M, M′ = Al, Zr, Ti, Si and R, R′ = Et, Pr, ^{i}Pr, ^{t}Bu.

(12) Hollemann, A. F.; Wiberg, E.; Wiberg, N. *Lehrbuch der Anorganischen Chemie*; Walter de Gruyter-Verlag: Berlin, New York, 1985.
(13) Li, C. P.; Chen, Y. W.; Yen, T. M. *J. Sol Gel Sci. Technol.* **1995**, *4*, 205.
(14) Levy, R. M.; Bauer, D. J. *J. Catal.* **1967**, *9*, 76.
(15) Scharper, H.; Doesburg, E. B. M.; Van Reijen, L. L. *Appl. Catal.* **1983**, *7*, 211.
(16) Ozawa, M.; Kimura, M.; Isogai, A. *J. Less-Common Met.* **1990**, *162*, 297.
(17) Burtin, P.; Brunelle, J. P.; Pijolat, M. *Appl. Catal.* **1987**, *34*, 225.
(18) Ozawa, Y.; Fujii, T.; Tochihara, Y.; Kanazawa, T.; Sagimori, K. *Catal. Today* **1998**, *45*, 167.
(19) Ozawa, M.; Kato, O.; Suzuki, S.; Hattori, Y.; Yamamura, M. *J. Mater. Sci. Lett.* **1996**, *15*, 564.
(20) Arai, H.; Machida, M. *Appl. Catal. A Gen.* **1996**, *138*, 161.
(21) McVicker, G. B.; Garten, R. L.; Baker, R. T. K. *J. Catal.* **1978**, *54*, 129.
(22) Church, J. S.; Cant, N. W. *Appl. Catal.* **1993**, *101*, 105.
(23) Engelhardt, G.; Michel, D. *High-resolution solid-state NMR of silicas and zeolites*; Chichester: New York, 1987.

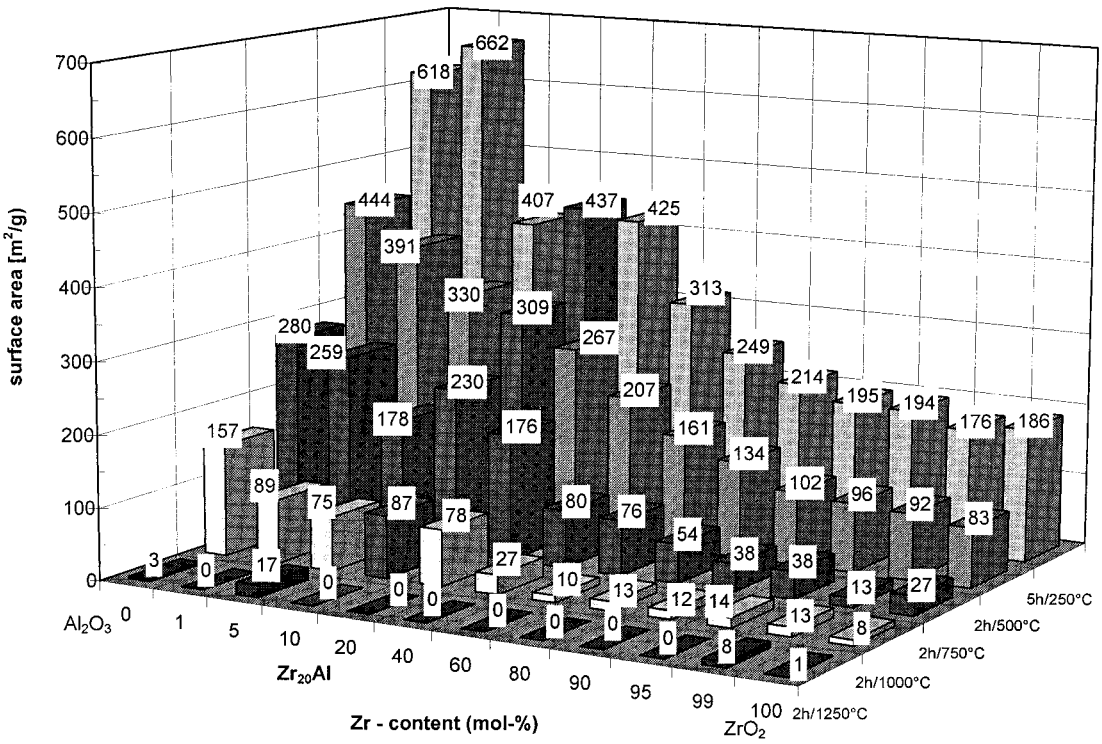

Figure 1. Single point BET-surface areas of Al−Zr mixed oxides in dependence of composition and calcination temperature.

By this hydrolysis−co-condensation−reaction ZrO_2−Al_2O_3 mixed oxides have been synthesized covering the whole composition range. Acid-catalyzed conditions have been chosen to avoid the domain formation typical for base-catalyzed sol−gel conditions. An advantage of the method applied is that stabilizing agents and/or catalytically active components can be incorporated easily during the sol−gel-based preparation step. The materials are named amorphous mixed oxides AM-Zr_xAl, where *x* stands for the mol % content of the minor component., i.e., AM-$Zr_{20}Al$ is a mixed oxide composed of 20 mol % ZrO_2 and 80 mol % Al_2O_3.

The as-synthesized materials were calcined previously at 250 °C. Single-point BET was used to estimate the surface area. Then the materials were calcined at increasingly higher temperatures up to 1250 °C to obtain first information on the thermal stability of their porosity. The effect of calcination temperature on the BET-surface area in dependence of composition is shown in Figure 1.

While the pure sol−gel-derived alumina has the highest total surface area, when calcined at 500 °C (444 m^2/g, left corner) or higher, the pure zirconia, made by exactly the same procedure, shows only 186 m^2/g, although considering the higher molecular weight of zirconia a surface area of about 250 m^2/g was expected. This indicates a slightly denser microstructure in the case of the zirconia. This general trend also holds for the other materials, total surface area drops with increasing zirconia content, while the most drastic area loss occurs at the lower ZrO_2 contents (407 m^2/g at 1% ZrO_2).

In general the surface area decreases as expected with increasing calcination temperature for all materials. When we consider, that commercial ZrO_2 powders have surface areas below 50 m^2/g, the surface area of 100−

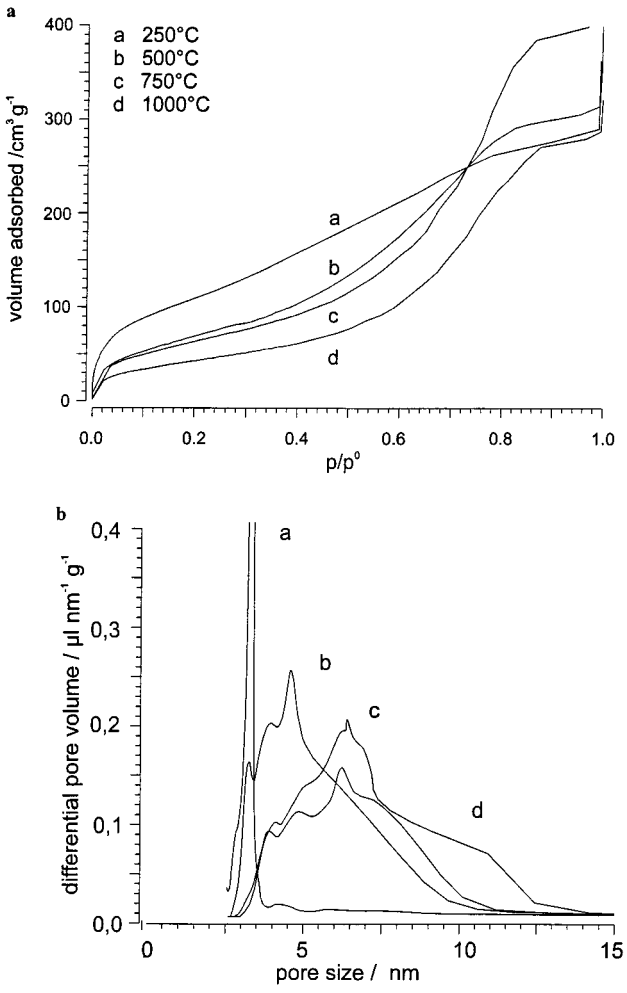

Figure 2. Effect of calcination temperature on Ar adsorption isotherms (a) and pore size distributions (b) of AM-$Zr_{20}Al$

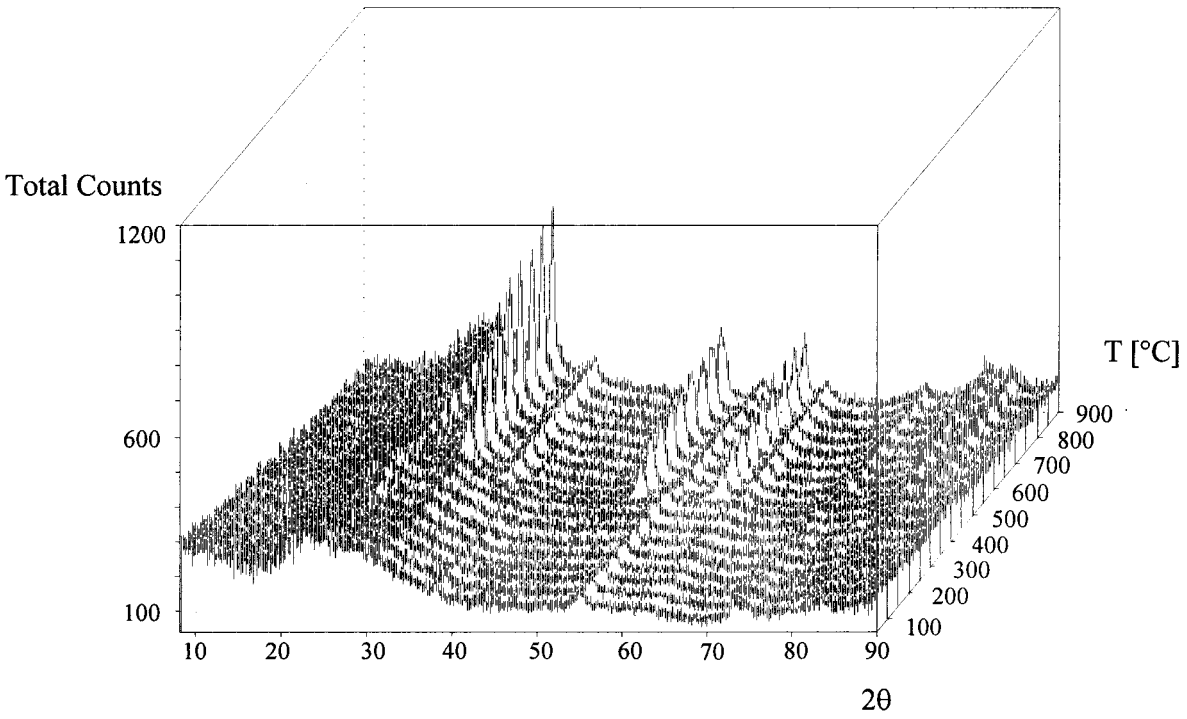

Figure 3. Effect of increasing temperature on the X-ray diffraction pattern of AM-$Zr_{80}Al$

160 m^2/g for the ZrO_2-rich mixed oxides treated at temperatures up 500 °C, is remarkable. Only the mixed oxides with less than 20 mol % ZrO_2 keep very high surface areas even at the more severe conditions of 1000 °C. After treatment at 1250 °C, all materials have lost most of their porosity and surface area (<10 m^2/g).

Interesting are the materials continuing 80−100 mol % ZrO_2, which show quite similar surface areas after the various temperature treatments from 250 to 750 °C. The total amount of alumina apparently does not affect the sintering behavior of the zirconia. Worth mentioning is the behavior of the first five samples of low zirconia content (0−20% ZrO_2), all of which show thermal stability up to 750 °C with surface areas in the rage of 180−260 m^2/g. Even after treatment at 1000 °C the remaining surface areas of 75−90 m^2/g are still high. From the materials with high surface area the material with the highest zirconia content, AM-$Zr_{20}Al$, was selected for further investigations.

The development of the pore structure with increasing temperature was investigated by argon adsorption isotherms in liquid argon.[24] Figure 2a shows the isotherms of the mixed-oxide AM-$Zr_{20}Al$ at different temperatures; Figure 2b, the related pore size distributions for this material.

As is evident from Figure 2a, all these materials are mesoporous. Each sample shows a hysteresis typical for "bottleneck" mesopores.[25] The pore size distributions (Figure 2b), calculated from the desorption branch by the method of Dollimore−Heal,[26] are also strongly affected by the calzination temperature. While a very narrow pore size distribution around 3.4 nm exists at 250 °C for the AM-$Zr_{20}Al$ (Figure 2b), at higher temperatures a broad distribution (6.6 nm) and a reduced adsorbed volume are observed, indicative of a partial collapse of the pore structure, probably by breaking down pore walls between smaller pores. Table 1 compares the surface areas and the pore diameters of selected materials after the different calcination temperatures. The pure Al_2O_3 shows broad pore distributions, where pore size increases with temperature. The incorporation of 20 mol % ZrO_2 into the Al_2O_3 matrix seems to cause a general decrease in pore size. At 750 °C and 1000 °C, the pure alumina sample has twice the mean pore diameter (12.01 nm) relative to the AM-Zr_{20}-Al (6.34 nm). In Table 1, all results are summarized.

Table 1. BET Areas and Average Pore Sizes for Selected Sol−Gel Materials

material	calcination temperature	BET surface area (m^2/g)	average pore size (nm)
Al_2O_3	250 °C, 5 h	662	5.10
	500 °C, 2 h	391	6.66
	750 °C, 2 h	259	12.01
	1000 °C, 2 h	89	15.20
ZrO_2	250 °C, 5 h	186	2.79
	500 °C, 2 h	83	2.98
	750 °C, 2 h	27	11.51
	1000 °C, 2 h	8	–
$Zr_{20}Al$	250 °C, 5 h	425	3.36
	500 °C, 2 h	267	4.50
	750 °C, 2 h	176	6.34
	1000 °C, 2 h	78	6.60

A possible explanation for the narrow poresize distribution at 250 °C for the AM-$Zr_{20}Al$ can be that the complexing agent hydroxypentadione acts like a template in analogy to MCM materials.[27]

To obtain further information about the porosity changes documented by the adsorption isotherms, a powder X-ray diffraction pattern has been obtained. The effect of increasing temperature on the microstructure

(24) Storck, S.; Bretinger, H.; Maier, W. F. *Appl. Catal. A Gen.* **1998**, *174*, 137.
(25) Lowell, S.; Shields, J. E. *Powder surface area and porosity*; Chapman & Hall: New York, 1991.
(26) Dollimore, D.; Heal, G. R. *J. Appl. Chem.* **1964**, *14*, 109.
(27) Zhao, X. S.; Lu, G. Q. M.; Millar, G. J. *Ind. Eng. Chem. Res.* **1996**, *35*, 2075.

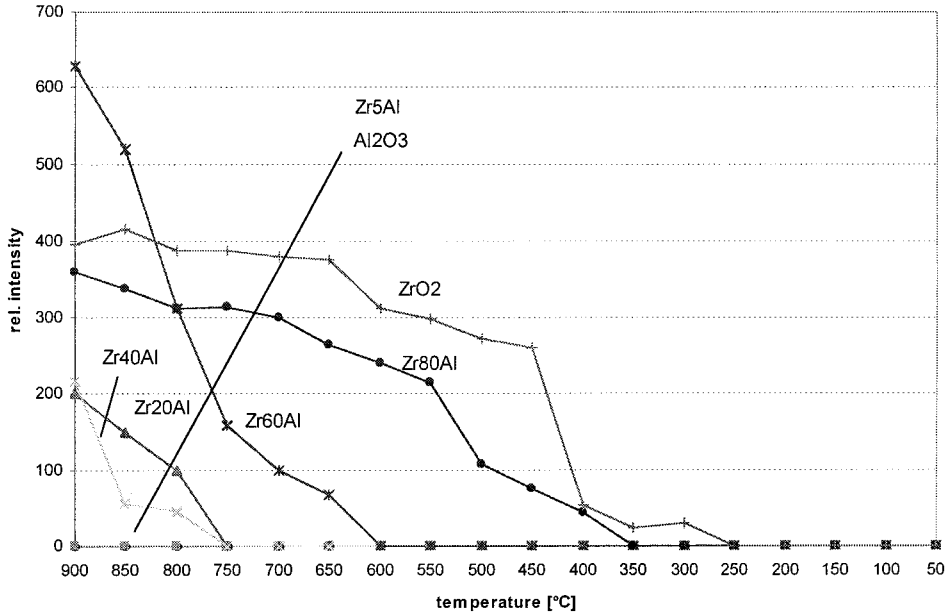

Figure 4. Dependence of the intensity of the (111) reflex of t-ZrO_2 on composition of AM-Zr_xAl and temperature, obtained from temperature-dependent X-ray diffraction measurements.

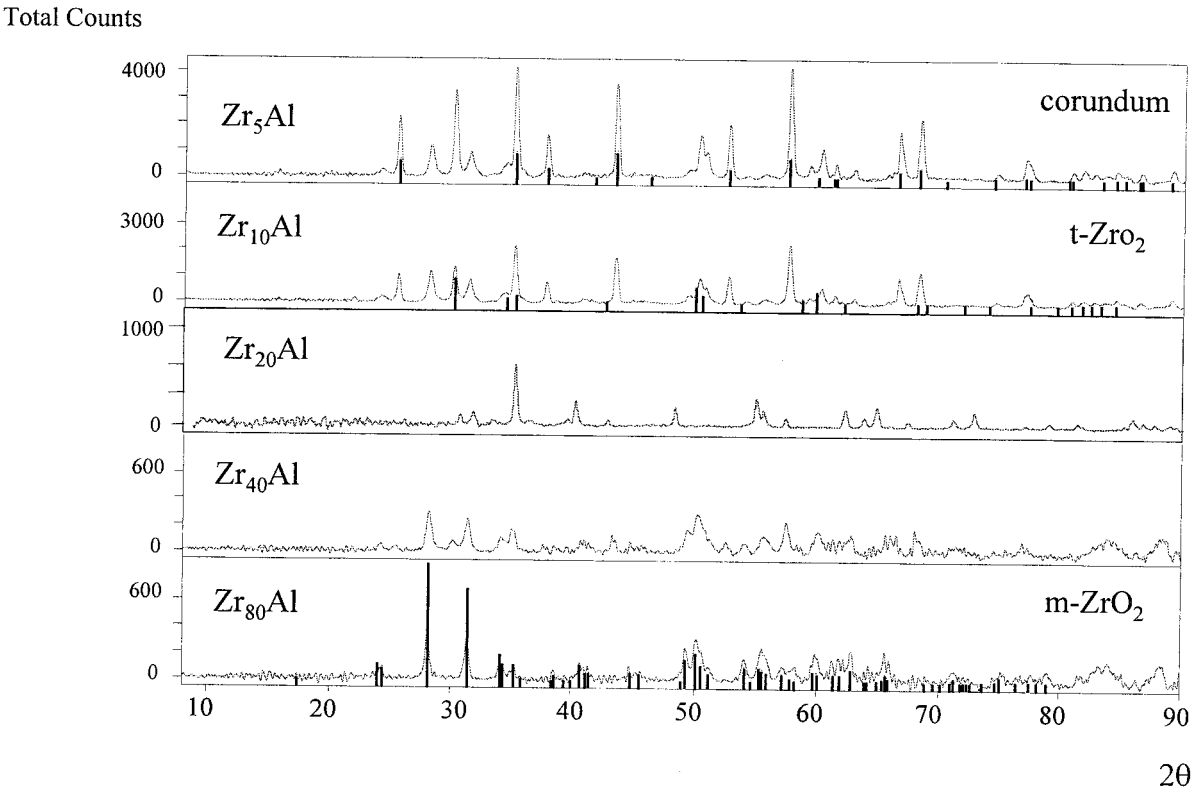

Figure 5. Assignment of identified phases in selected X-ray diffraction pattern of AM-Zr_xAl

of the AM-$Zr_{80}Al$ sample, calcined at 250 °C, is shown in Figure 3 by temperature-dependent powder X-ray diffraction. While the material is X-ray amorphous at temperatures up to 350 °C, the tetragonal phase of ZrO_2 starts to form at higher temperatures. No indication for the formation of corundum or monoclinic ZrO_2 was obtained at temperatures below 1000 °C. Although a single phase can be identified, the broad half-width and low total intensities of the reflexes are indicative of small crystallites.

In Figure 4, the temperature dependence up to 900 °C of the evolution of the intensities of the [111] reflex (at $2\theta = 30°$) of t-ZrO_2 is shown for selected compositions. Compared to the pure ZrO_2, which shows crystallization at 300 °C, crystallization is shifted to higher temperatures with increasing Al content. However, even with 60 and 80% Al, crystallization cannot be avoided, even so temperatures of 750 °C are now required.

Mixtures <20% ZrO_2 stay amorphous over the whole temperature range and even the mixture AM-$Zr_{40}Al$ shows very little crystallinity. This trend is confirmed with DSC (differential scanning calorimetry) measurements, where clear exothermic changes are detected for the following materials at the temperatures indicated:

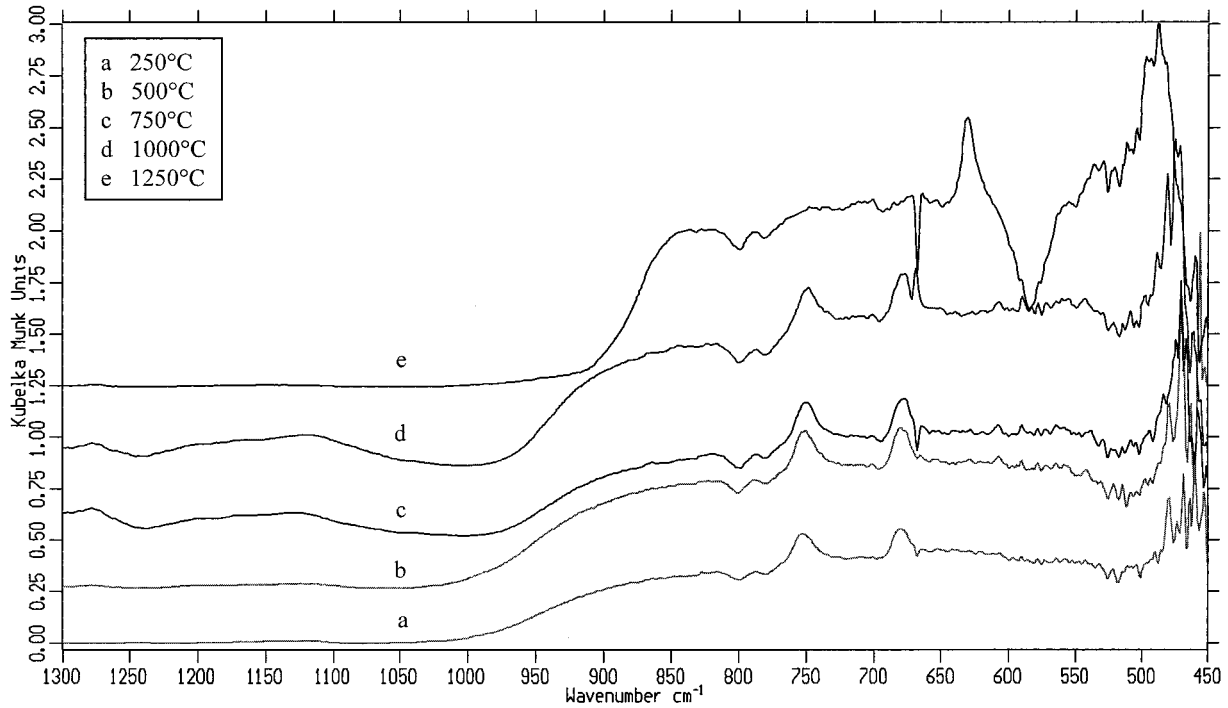

Figure 6. Effect of calcination temperature on the IR spectra (DRIFT) of AM-Zr_{20}Al

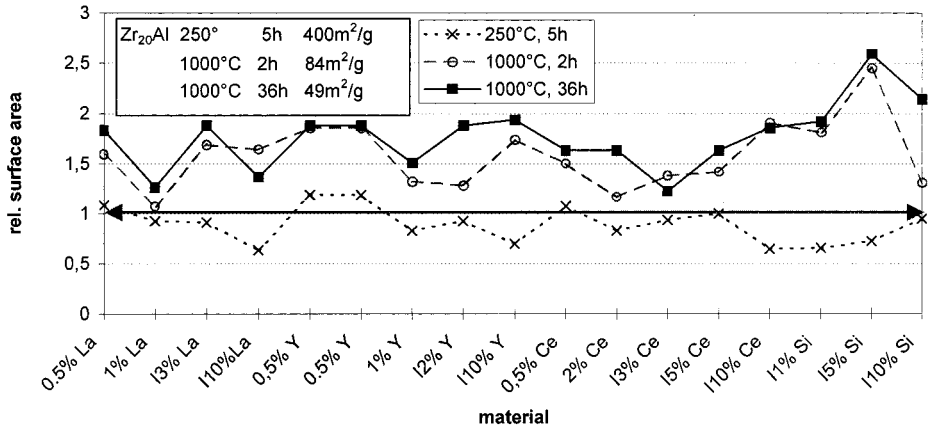

Figure 7. Effect of calcination temperature on the single point BET surface area of stabilized AM-Zr_{20}Al. Nature of doping ions and concentrations are indicated.

ZrO_2, 489 °C; AM-Zr_{99}Al, 495 °C; AM-Zr_{95}Al, 502 °C; AM-Zr_{80}Al, 561 °C.

All the other compositions do not show any crystallization effect in accord with DSC up to 700 °C, confirming that the crystallinity in AM-Zr_{20}Al, AM-Zr_{40}Al, and AM-Zr_{60}Al is very low.

The relatively high surface area as well as the low crystallinity after temperature treatments at 900 and 1000 °C prompted another calcination of the selected AM-materials at 1250 °C in the oven. In Figure 5 the X-ray diffraction patterns of the samples after treatment at 1250 °C are shown together with selected database JCPDS pattern. The JCPDS pattern (bar pattern) are identified in the upper right corners. There is very little crystallization in AM-Zr_{40}Al and AM-Zr_{80}Al. In AM-Zr_5Al, all three phases are present, whereby corundum and t-ZrO_2 dominate. The corundum formation decreases with increasing zirconia content. Apparently migration of alumina is supressed with increasing ZrO_2. In AM-Zr_{80}Al, surprisingly little crystalline ZrO_2 is detectable, indicating an effective stabilization of the amorphous ZrO_2-phase by the Al. The tetragonal ZrO_2 is present only in the materials with high Al content. With increasing ZrO_2 content the monoclinic phase increases and at compositions >40% ZrO_2 only m-ZrO_2 forms. The monoclinic zirconia seems to suppress the other crystalline phases. Although in all materials the amorphous phase seems to dominate, most surface area was lost in all samples after this high temperature treatment at 1250 °C (see Figure 1), indicating that the loss of surface area should not be assigned exclusively to crystallization, but to general sintering phenomena.

Infrared Spectroscopy. Diffuse reflectance IR (DRIFTS) measurements were obtained, at various calcination temperatures, for the AM-Zr_{20}Al material, shown in Figure 6.

The IR bands do not change in the temperature range 250−750 °C, but at 1000 °C a small band around 655 cm^{-1} is formed, while after calcination at 1250 °C the spectrum changes significantly. Between 250 °C and 1000 °C, the two characteristic bands at 680 and 750 cm^{-1} can be associated to Al−O[13] and Zr-O bonds.[28] In

the region around 470 cm^{-1} the adsorption band of Zr−O appears,[29] assigned to the tetragonal phase. This peak shifts with temperature to 490 cm^{-1} and splits to a second band at 540 cm^{-1}. These bands can be associated to the phase transformation of zirconia to the monoclinic form.[30] After calcination at 1250 °C, a new, sharp band is formed at 630 cm^{-1}, in analogy to what has been reported for corundum by Vazquez and Li and other authors.[13,28,31] A new band appears between 570 and 500 cm^{-1}, which is attributed to the monoclinic ZrO_2 phase.[32]

For the weak band at 790 cm^{-1} in each spectra no assignments were found in the literature. We propose therefore a Zr−O−Al stretch frequency. The DRIFTS investigations confirm the above-described X-ray measurements. Both techniques indicate that there is no significant phase change or phase separation up tp 1000 °C, but after calcination at 1250 °C the spectra change drastically due to phase separations, crystallization of the amorphous alumina as corundum phase, and the conversion of the tetragonal zirconia into the monoclinic phase.

Stabilization. After the temperature effects on the stability and phase separations of the sol−gel materials had been mapped out, the stabilization of the selected mixed oxide AM-$Zr_{20}Al$ was investigated. The stabilizing effect of La^{3+}, Y^{3+}, and Ce^{3+} on the porosity of the material was studied. The sol−gel preparation procedure allowed the effect of these ions to be studied by adding them to the sol (co-polycondensation), resulting in a bulk distribution of these ions and comparing these effects to those of conventional impregnation approaches. Figure 7 gives an overview of the effect of these ions, normalized to the surface areas of the unstabilized AM-$Zr_{20}Al$ at the corresponding temperature.

While all the doped materials after calcination at 250 °C show surface areas comparable to those of the pure mixed oxide (dotted line), a significant effect is observed after treatment at 1000 °C resulting in a doubling of total surface area.

The stabilization with La^{3+} is successful by impregnation with a small La^{3+} content. Impregnating with 3% La^{3+} nearly doubles the surface area after 36 h at 1000 °C. With increasing La^{3+} content, the stabilizing effect of the impregnation decreases, while the incorporation of La^{3+} has nearly no stabilizing effect.

For Y^{3+}, we see a different behavior. Especially small amounts, independent of impregnation or incorporation, stabilize the surface area (doubling).

With Ce^{3+}, the stabilization effect decreases with increasing incorporation, while it increases with increasing amount by impregnation approaching a doubling of the surface area with 10% Ce^{3+}.

Nevertheless, the best results have been obtained by impregnating with 5% Si^{4+}, an additive just recognized once for its stabilizing effects.[33] While the impregnated samples have a reduced surface area at 250 °C (probably due to pore filling and reduction of the pore volume), this SiO_2 film stabilizes this pore system against collapse even after 36 h at 1000 °C. A remarkable surface area of 206 m^2/g is observed and after 36 h at 1000 °C 127 m^2/g still remain.

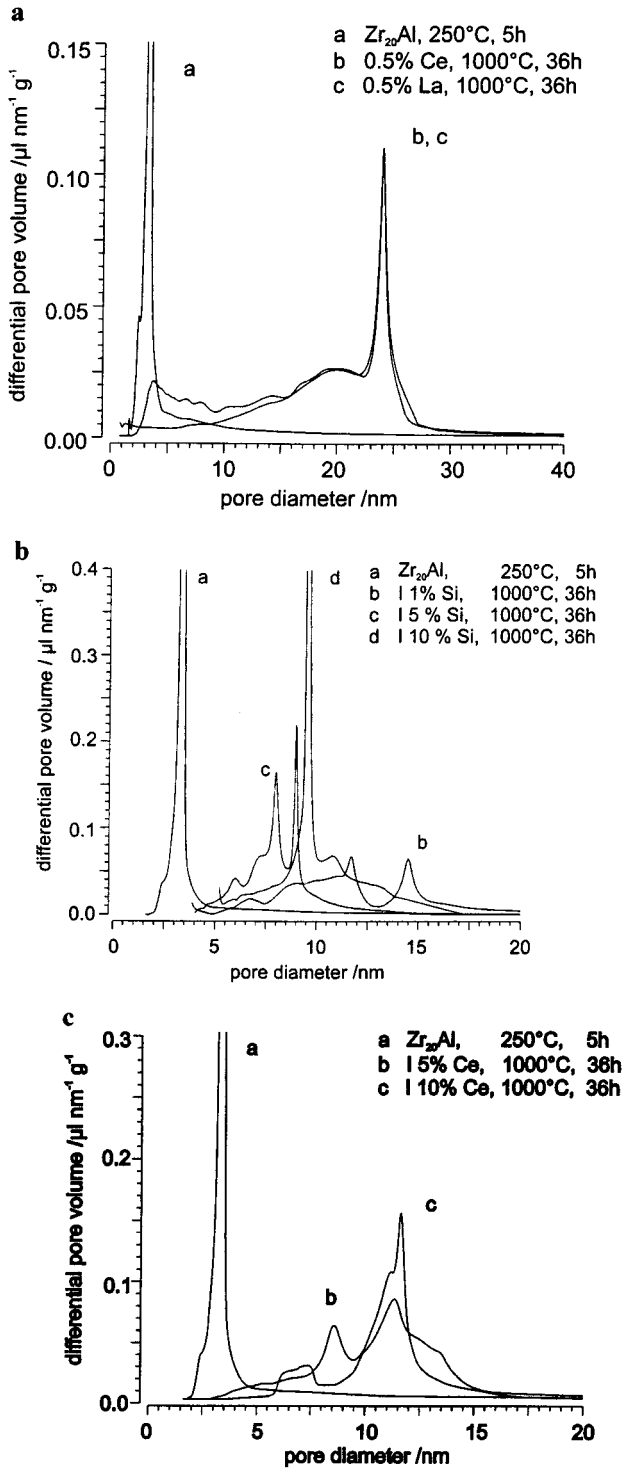

Figure 8. Effect of selected dopant ions on the pores size distributions (calculated from Ar desorption by the method of Dollimore-Heal[26]) of AM-$Zr_{20}Al$. Dopants and calcination temperature are indicated.

Figure 8a−c shows the pore size distribution of selected stabilized samples after 36 h at 1000 °C, in comparison to the basic unstabilized material at 250 °C.

In comparison to Figure 2b, it is evident, that the pore size increases to diameters around 10 nm, but these are

(28) Lee, J. S.; Park, J. I.; Choi, T. W. *J. Mater. Sci.* **1996**, *31*, 2833.
(29) Debsidkar, C. *J. Non-Cryst. Solids* **1986**, *86*, 231.
(30) Debsidkar, C. *J. Non-Cryst. Solids* **1986**, *87*, 343.
(31) Vázquez, A.; López, T.; Gómez, R.; Bokhimi, Morales, A.; Novaro, O. *J. Solid State Chem.* **1997**, *128*, 161.
(32) Phillippi, C. M.; Mazdiyashi, K. S. *J. Am. Ceram. Soc.* **1970**, *54*, 254.
(33) Horiuchi, T.; Sugiyama, T.; Mori, T. *J. Mater. Chem.* **1993**, *3*, 861.

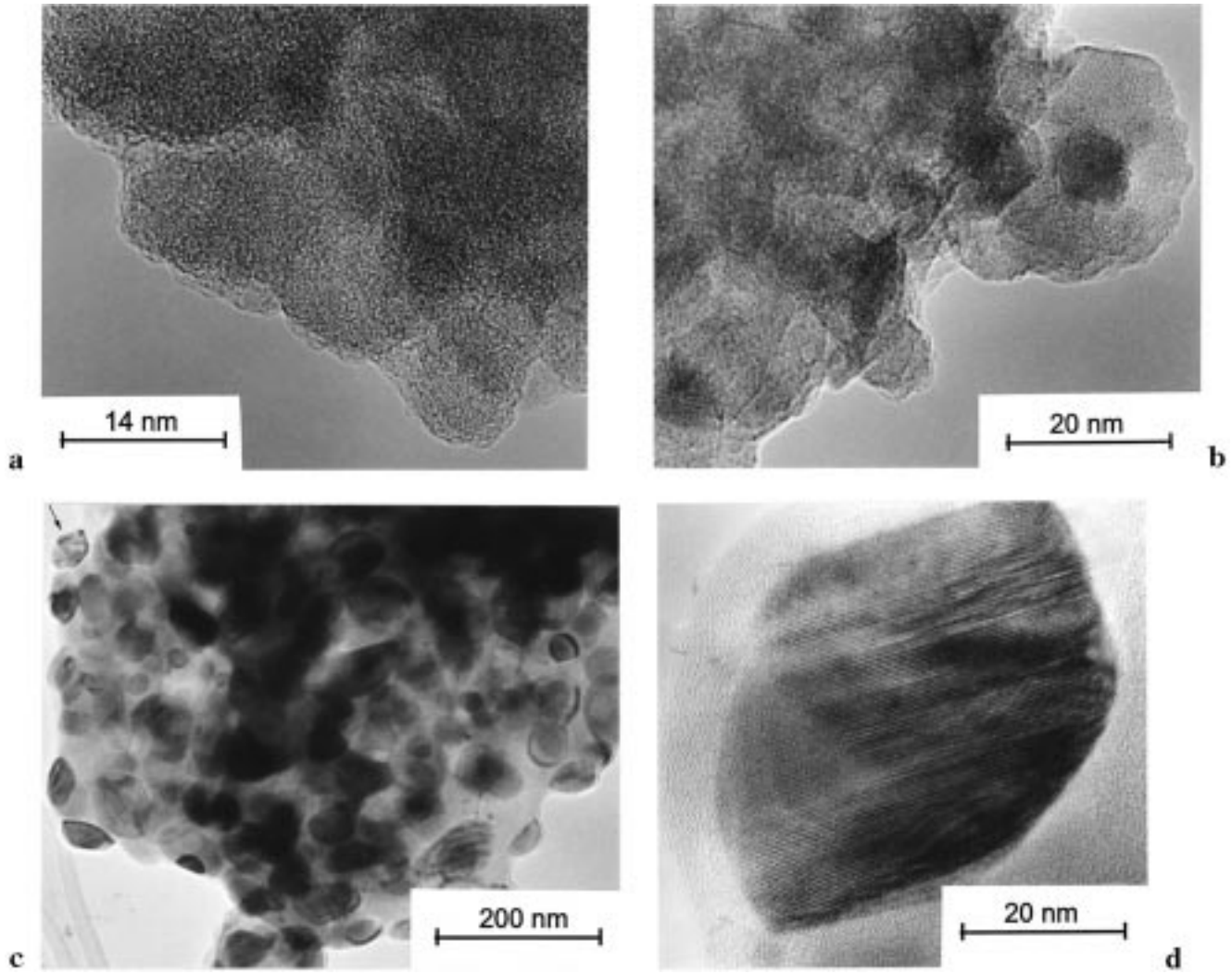

Figure 9. TEM micrographs of AM-Zr_{20}Al after calcination at 750 °C, 1000 °C, and 1250 °C.

not as broad as in the unstabilized sample. Although the samples have been treated 36 h longer at 1000 °C, there is no pore broadening comparable to that in Figure 2b. The samples impregnated with 1% and 5% Si^{4+} show bimodal-like distributions. The sample impregnated with 10% SiO_2 has a very narrow distribution, but a smaller pore volume, what may explain the smaller surface area.

Figure 8b displays the results for the impregnation with Ce^{3+}.

By impregnation with Ce^{3+} the pore diameter is shifting to ~12−13 nm, around 2 nm more than the Si^{4+} impregnated samples. Again we see the effect better with more ceria, so the impregnation with 10% CeO_2 shows a more narrow distribution with a higher pore volume.

Compared to the incorporation attempts (Figure 8c), the results in the stabilization effects are understandable. Either the incorporation of a small amount of Ce^{3+} either 0.5% La^{3+} leads to a nearly identical pore size distribution in the macroporous region around 24 nm. While impregnation stabilizes the pore diameters around 10−12 nm, the incorporation results in macropores around 25 nm. This can perfectly explain the differences in the surface areas of the stabilized samples (Figure 6). But comparing the incorporation of 0.5% Ce^{3+} (curve b, Figure 8c) with the impregnation with 5% Ce^{3+} (curve b, Figure 8b), it is evident that they stabilize the basic material in the same manner, even though the pore diameters differ with the factor 2. Only the broadness in the incorporated material is smaller; the distribution is sharper than by impregnation. By far the highest stabilization was obtained with AM-Zr_{20}Al, stabilized by impregnation with 5 mol %TEOS and calcined for 2h at 1400 °C. After this high-temperature treatment this material still showed a total surface area of 82 m^2/g.

^{27}Al CP MAS NMR. The sample AM-Zr_{20}Al has been measured directly after the preparation and aging at room temperature, after calcination at 250 °C and at 1000 °C. In all these spectras, a sharp peak at a chemical shift 0 ppm with a shoulder at 50 ppm can be found. Therefore the biggest part of the Al_2O_3 is present in 6-fold coordination, a small amount has the coordination number 4. The peak form is not changing in the whole temperature range from room temperature up to 1000 °C. The aluminum environment is not changing at all. A control measurement of corundum results in same peak distribution in the spectrum. It can be summarized, that the 20 mol % ZrO_2 in the mixed oxide AM-Zr_{20}Al have no influence on the aluminum coordination in the matrix.

HRTEM/EDX. Some selected TEM pictures obtained from sample AM-Zr_{20}Al are shown in Figure 9:

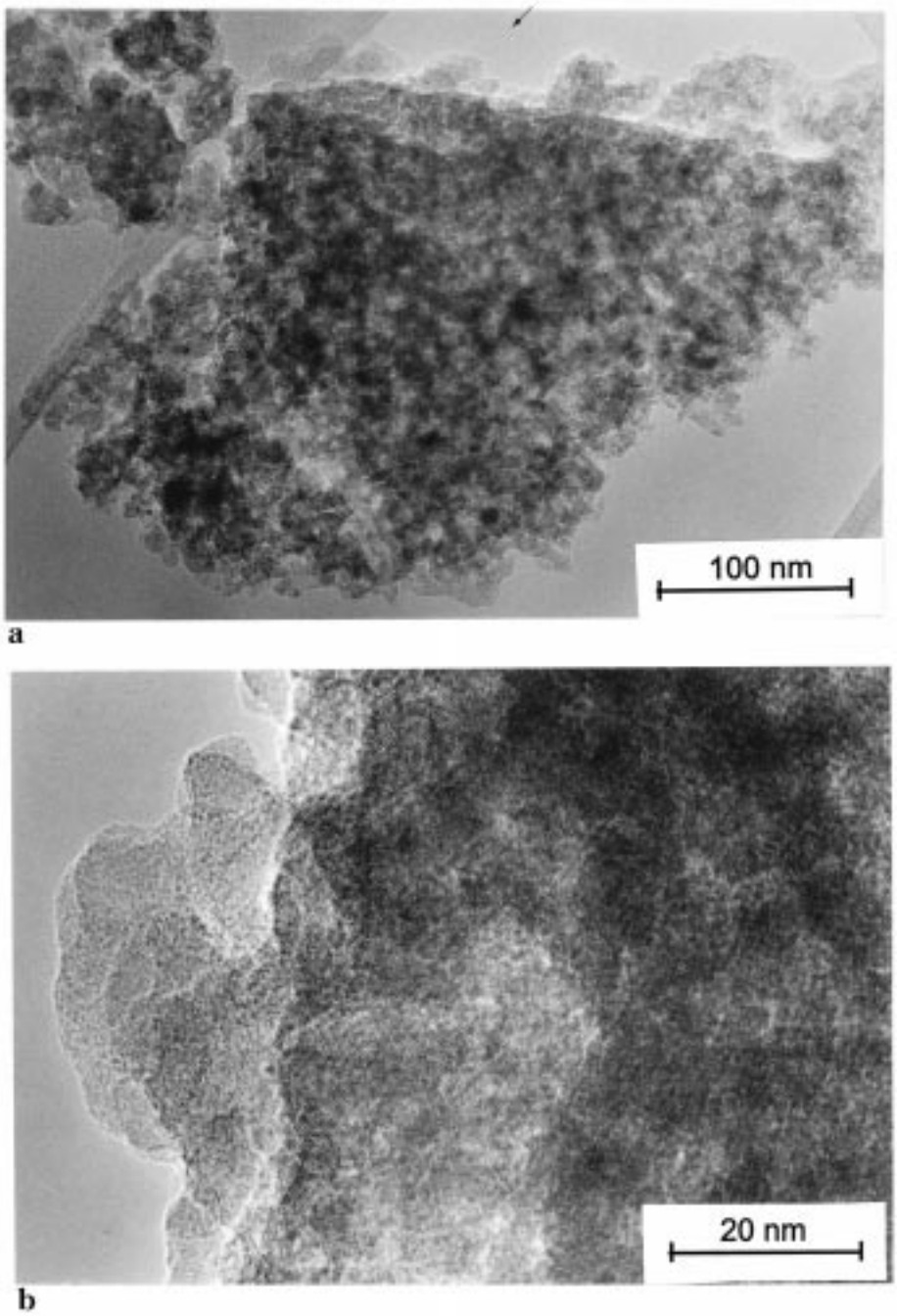

Figure 10. TEM micrographs of AM-$Zr_{20}Al$, impregnated with 1 wt % Si, after calcination at 1400 °C.

The AM-$Zr_{20}Al$ pretreated to 750 °C shows only an amorphous nature and a homogeneous elemental distribution (Figure 9a). The homogeneous elemental distribution of Al and Zr in the mixed oxide at a molar ratio of 2:8 was confirmed by selected area EDX. All areas analyzed (from 2 nm diameter up to several hundred nm) show identical chemical composition indicative of the absence of domains. After calcination at 1000 °C (Figure 9b), darker and lighter regions in the micrograph can be recognized. The EDX analysis shows an increase of the Zr content for the darker parts and a slight increase of the Al content in lighter regions. Apparently the sample shows first signs of phase separation and starts to lose its homogeneity. But there are still only few signs of crystallinity, the amorphous nature still dominates the material. After the next calcination step at 1250 °C, phase separation has progressed and crystalline particles can be identified throughout the material (Figure 9c). At higher magnification (Figure 9d) the lattice fringes of large crystallites, 30−60 nm in diameter, can be identified, embedded in a still amorphous matrix. EDX analysis of the crystallites reveals that most of them are ZrO_2, while the amorphous embedding matrix is mainly composed of Al_2O_3. This agrees rather well with the X-ray diffraction data, where crystalline ZrO_2, already dominates the diffraction pattern, while the corundum content is significantly reduced relative to the AM-$Zr_{10}Al$.

In Figure 10 the micrographs of AM-$Zr_{20}Al$, stabilized by impregnation with 5 mol % TEOS and calcined for 2 h at 1400 °C are shown. Figure 10a gives an overview of a typical particle, already indicating an amorphous

microstructure. This is confirmed by the high-resolution micrograph (Figure 10b) where no crystalline nanostructures are detectable. The morphology of this sample, heated to 1400 °C, is comparable to that of the unstabilized sample after calcination at 250 °C. A series of selected area EDX-analyses shows a rather consistent composition of Al:Zr = 8:2, with no indication of significant elemental separation. This is remarkable, since it indicates that even amorphous porous oxides can exhibit extraordinary thermal stability, if composed properly. Since nothing is known about the thermal stability of amorphous mixed oxides at high temperatures, this finding may open the door to new classes of temperature-stable materials.

Conclusions

With a modified sol−gel process nearly domain free amorphous mixed Zr−Al mixed oxides can be prepared covering the whole range of composition. The materials show a high porosity, especially the materials high in Al content show surface areas up to 600 m^2/g. While most materials lose the surface area, phase separate and crystallize rapidly with increasing temperatures, the materials with lower Zr content show significant thermal stability and surface areas up to 80 m^2/g were maintained after treatment at 1000 °C. Impregnation as well as incorporation of a variety of common metal ions did not result in the expected thermal stabilization. By subsequent impregnation of the materials with TEOS, surface areas up to 200 m^2/g were maintained even after treatment at 1250 °C for 2 h. It was found that even after calcination at 1400 °C a surface area of 82 m^2/g were observed, while elemental distribution and homogeneous character were maintained even at atomic resolution. Apparently, phase separation and crystallization of materials can be slowed drastically by the appropriate chemical composition stabilizing the amorphous nature even at very high temperatures. Key design element is most likely the rather homogeneous elemental distribution resulting from the acid-catalyzed sol−gel process applied. The stability of such materials under combustion conditions has to be studied. We have shown that amorphous mixed oxides may be a promising new approach to the development of high-temperature stable porous materials.

Acknowledgment. We thank C. Lettmann for the electron microscopic investigations, A. Rufińska for the ^{29}Al-MAS-NMR investigations and S. Palm for the X-ray diffraction measurements. W.F.M. thanks the Fonds der Chemischen Industrie for continuing support.

CM990280L